Testing the Copernican Principle Via Cosmological Observations

Krzysztof Bolejko[1,2] and J. Stuart B. Wyithe[1]

[1]School of Physics, The University of Melbourne, VIC 3010, Australia
[2]Nicolaus Copernicus Astronomical Center, Bartycka 18, 00-716 Warsaw, Poland

E-mail: bolejko@camk.edu.pl, swyithe@unimelb.edu.au

Abstract. Observations of distances to Type-Ia supernovae can be explained by cosmological models that include either a gigaparsec-scale void, or a cosmic flow, without the need for Dark Energy. Instead of invoking dark energy, these inhomogeneous models instead violate the Copernican Principle. we show that current cosmological observations (Supernovae, Baryon Acoustic Oscillations and estimates of the Hubble parameters based on the age of the oldest stars) are not able to rule out inhomogeneous anti-Copernican models. The next generation of surveys for baryonic acoustic oscillations will be sufficiently precise to either validate the Copernican Principle or determine the existence of a local Gpc scale inhomogeneity.

Keywords: dark energy theory, supernova type Ia

PACS numbers: 98.80-k, 95.36.+x, 98.65.Dx

1. Introduction

The Copernican Principle states that we do not occupy any special place in the Universe. The Friedmann–Lemaître–Robertson–Walker (FLRW) models are built on this principle, and provide a remarkably precise description of cosmological observations [1, 2, 3]. One could therefore think of this as an indirect demonstration of the Copernican Principle. However, homogeneous and isotropic FLRW models are not the only solutions of Einsteins equations which are able to fit cosmological observations. In particular, a number of inhomogeneous models have been proposed, each of which are able to describe the evolution of distance with redshift as measured via type-Ia supernova (SnIa) without need of a cosmological constant [4, 5, 6, 7, 8] (see [9] for a review). Moreover, these models may be constructed in such a way that they describe the details of the cosmic microwave background power spectrum (CMB) [5, 6]. By eshuing the constraint of inhomogeneity, these inhomogeneous models violate the Copernican Principle and suggest that we live near the center of a large (of several gigaparsecs diameter) highly isotropic void.

Inhomogeneous models are able to fit a variety of sets of cosmological observations without containing a cosmological constant because the lack of homogeneity offers

a great degree of flexibility [10]. For example, since the last scattering surface is separated from regions where supernova are observed by great distances, the property of inhomogeneity allows a model to be constructed which provides different physical densities in the regions from which these two sets of observational data are drawn. Thus, what is required to constrain inhomogeneous solutions to the apparent acceleration of the Universe includes several sets of data that measure a range of observables at comparable redshifts. In this paper we confront two general classes of inhomogeneous, dark energy free models with observations of SnIa, with measurements of the baryon acoustic oscillations (BAO), and with the variation of the Hubble parameter with redshift. All these observational data are drawn from $z < 1.8$. We begin by describing the Lamaître–Tolman model (the simplest spherically symmetric inhomogeneous generalization of FLRW model), and then construct a range of 2-parameter models to describe a local large scale inhomogeneity. We then discuss constraints on the scale of these inhomogeneities based on existing and forthcoming data.

2. The Lemaître–Tolman model

The Lemaître–Tolman (LT) model [11] is a spherically symmetric, pressure free, irrotational solution of the Einstein equations. Its metric has the form

$$\mathrm{d}s^2 = c^2\mathrm{d}t^2 - \frac{R'^2(r,t)}{1+2E(r)}\,\mathrm{d}r^2 - R^2(t,r)\mathrm{d}\Omega^2, \tag{1}$$

where $\mathrm{d}\Omega^2 = \mathrm{d}\theta^2 + \sin^2\theta\mathrm{d}\phi^2$. Because of the signature $(+,-,-,-)$, the $E(r)$ function must obey $E(r) \geq -1/2$. Here a prime ($'$) denotes ∂_r.

The Einstein equations reduce to the following two

$$\kappa\rho(r,t)c^2 = \frac{2M'(r)}{R^2(r,t)R'(r,t)}, \tag{2}$$

$$\frac{1}{c^2}\dot{R}^2(r,t) = 2E(r) + \frac{2M(r)}{R(r,t)} + \frac{1}{3}\Lambda R^2(r,t), \tag{3}$$

where $M(r)$ is another arbitrary function and $\kappa = 8\pi G/c^4$. Here a dot ($\dot{}$) denotes ∂_t. When $R' = 0$ and $M' \neq 0$, the density becomes infinite. This happens at shell crossings, and is an additional singularity to the Big Bang that occurs at $R = 0, M' \neq 0$. By setting the initial conditions appropriately the shell crossing singularity can be avoided (see [12] for detail discussion).

Equation (3) can be solved by simple integration:

$$\int_0^R \frac{d\tilde{R}}{\sqrt{2E + \frac{2M}{\tilde{R}} + \frac{1}{3}\Lambda\tilde{R}^2}} = c\left[t - t_B(r)\right], \tag{4}$$

where t_B appears as an integration constant and is an arbitrary function of r. This means that the big bang is not a single event as in the FLRW models, but occurs at different times at different distances from the origin. To define a particular LT model

two functions must be specified as initial conditions. For completeness we note that in the FLRW limit $R(r,t) = ra(t)$ [where $a(t)$ is the scale factor], $M(r) = M_0 r^3$, and $E(r) = -k_0 r^2$.

3. Parametrization of Inhomogeneous Models

In this paper we consider two families of models, in which the cosmological constant is set to zero ($\Lambda = 0$) and the observer is situated at the origin. The most popular way to explain SnIa without Λ is to postulate a large scale void centered near our position [4, 5, 6, 7, 8]. The density distribution at the current instant in this first family may be parametrized by (see Fig. 1)

$$\rho(t_0, r) = \rho_0 \left[1 + \delta_\rho - \delta_\rho \exp\left(-\frac{r^2}{\sigma^2}\right)\right], \tag{5}$$

where $\rho_0 = 0.3 \times (3H_0^2)/(8\pi G)$. In these models the big bang is assumed to occur simultaneously at every point ($t_B = 0$). The functions M and E are then calculated using eqs. (2) and (4) respectively.

A second possible explanation for the apparent acceleration observed using SnIa is inspired by the so called Hubble Bubble. In the Hubble Bubble phenomenon the expansion rate at distances beyond 100 Mpc is postulated to be slower than it is locally [13]. Such a phenomenon could be described by a second family of models parametrized using (see Fig. 1)

$$H_T(t_0, r) = \frac{\dot{R}}{R} = H_0 \left[1 - \delta_H + \delta_H \exp\left(-\frac{r^2}{\sigma^2}\right)\right]. \tag{6}$$

In these models density is assumed to be homogeneous at the current epoch. The function M can be calculated using the above relation and eq. (3). As can be easily checked, these two families of models are regular at the origin (for origin conditions in the LT models see [14]).

In each case the radial geodesics and redshift are calculated from [16]

$$\frac{\mathrm{d}t}{\mathrm{d}r} = -\frac{R'}{\sqrt{1+2E}}, \qquad \ln(1+z) = \int_0^r \mathrm{d}\tilde{r} \frac{\dot{R}'}{\sqrt{1+2E}}, \tag{7}$$

and the luminosity distance is $D_L = (1+z)^2 R$.

4. Cosmological Observations

In this paper we confront the inhomogeneous models described above with three sets of observations. Firstly, we consider observations of Type-Ia supernova, which are taken from the Union data set [17]. In addition we also present the constraints coming from the Riess gold data set [18], which until recently has been the most popular sample for testing inhomogeneous models. The second set of cosmological observations comprise measurement of the dilation scale of the BAO in the redshift space power-spectrum of

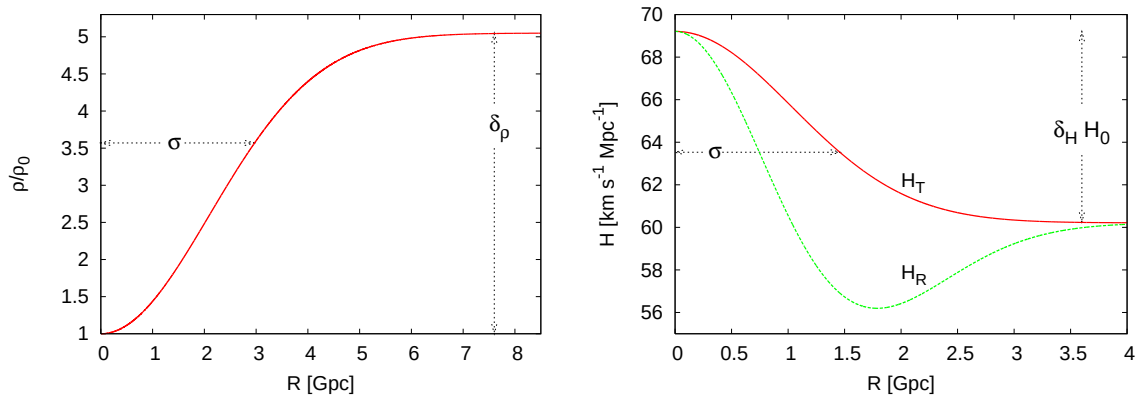

Figure 1. *Left* panel: The parametrization of the density distribution within the first family of model at the current instant. *Right* panel: The parametrization of the expansion rate (H_T) at the current instant within the second family of models, as well as the corresponding Hubble parameter H_R. The plotted profiles were obtained using parameters presented in Table 1.

46,748 luminous red galaxies (LRG) from the Sloan Digital Sky Survey (SDSS). The dilation scale is defined as

$$D_V = \left[D_A^2 \frac{cz}{H(z)} \right]^{1/3}, \tag{8}$$

where D_A is the comoving angular diameter distance and $H(z)$ is the Hubble parameter in function of redshift. The measured value of the dilation scale at $z = 0.35$ is 1370 ± 64 Mpc [19]‡. The Hubble parameter in equation (8) is related to expansion along the radial direction, and in the LT model is given by

$$H_R = \frac{\dot{R}'}{R'}. \tag{9}$$

In addition to the geometric measurements described above, the Hubble parameter has been estimated as a function of time based on the age of the oldest stars observed in galaxies at different redshifts [20]. Using eq. (7) it can be shown that within the LT model the Hubble parameter measured this way is also equal to H_R. Given a particular parametrization the null geodesic equations can be solved to calculate the luminosity distance, dilation scale and the Hubble parameter (H_R). These quantities can then be compared with observations to test the viability of the model by constraining parametrizations via a least square fit.

‡ It should be noted that the value of 1370 ± 64 Mpc was obtained within the framework of the linear perturbations imposed on a homogeneous FLRW background. It is still an open question whether such analysis is appropriate or should be carried out instead in the LT background. However, we proceed with the value for the D_V provided by Eisenstein et al. We will come back to this issue in Sec. 6.1 where we will try to partially estimate the errors which arise from application of different background models.

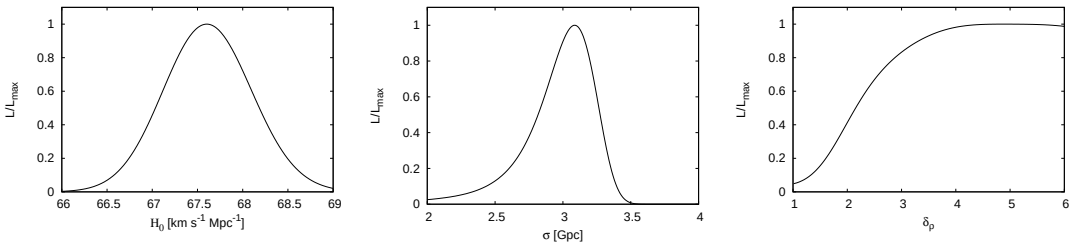

Figure 2. Likelihood profiles for H_0, σ, and δ_ρ based on the BAO+H(z)+Union data sets. *Left* panel: The H_0 likelihood profile obtained after marginalization over σ and δ_ρ. *Center* panel: The σ likelihood profile obtained after marginalization over H_0 and δ_ρ. *Right* panel: The δ_ρ likelihood profile obtained after marginalization over σ and H_0. The means are presented in Table 1.

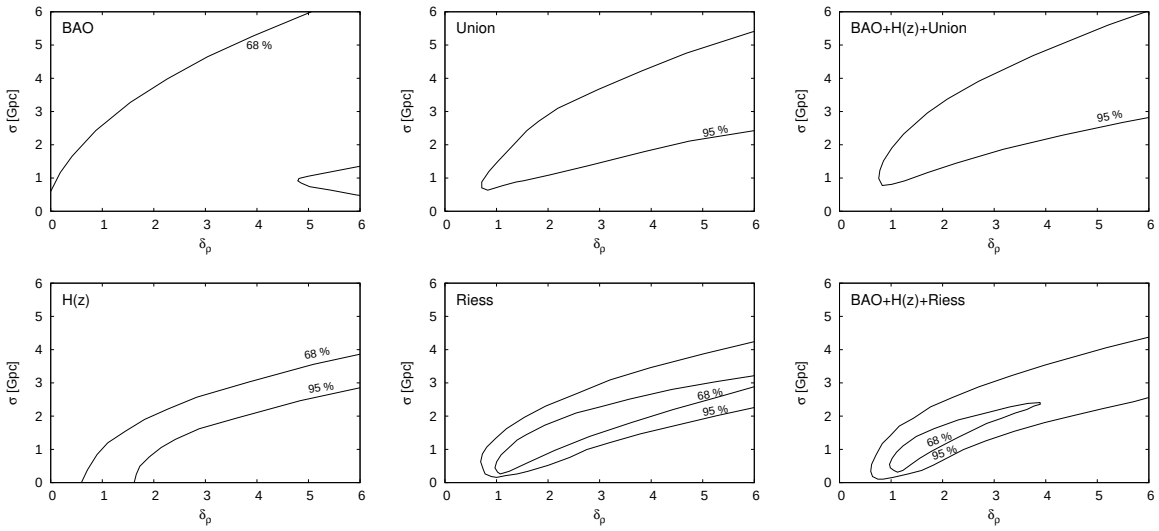

Figure 3. Observational constraints on the parameters of the first family of models (cosmic void models), shown as contour plots of χ^2 for the model given the data, after marginalizing over H_0. The confidence levels are set assuming a χ^2 distribution. *Upper Left*: constraints from the BAO. *Lower Left*: constraints from H(z). *Upper Center*: constraints from the Union data set. *Lower Center*: constraints from the Riess gold data set. *Upper Right*: joint constraints from the BAO+H(z)+Union data sets. *Lower Right*: joint constraints from the BAO+H(z)+Riess data sets.

5. Testing the Copernican Principle

5.1. Cosmic void models

We begin by constraining the first family of inhomogeneous models, characterized by $t_B = 0$. As can be seen from equation (5), the density increases from ρ_0 at the origin to $\rho = (1 + \delta_\rho)\rho_b$ at infinity. The left panel of Fig. 1 shows an example profile for which $\delta_\rho = 4.05$ and $\sigma = 2.96$. We note that the profile need not be extrapolated to infinity. Indeed, owing to the flexibility of inhomogeneous models the profile could

be modified arbitrarily at larger distances in order to fit other types of observations, including those of the CMB (see Appendix for more details). We allow the following three parameters to vary within specified ranges $H_0 \in [64, 76]$ km s^{-1} Mpc^{-1} , $\sigma \in [0, 6]$ Gpc, and $\delta_\rho \in [0, 6]$. The likelihood distributions for these parameters are presented in Fig. 2. The expected (mean) values derived from the likelihood profiles are presented in Table 1. The constraints on the parameters δ_ρ and σ are shown as contour plots of χ^2 after marginalizing over H_0 in Fig. 3. As can be seen the Union data set places tighter constraints on the models than the Riess data set. However, it should be emphasized that the uncertainties in the Union data set used here do not include systematic errors, which may be present owning to the joining of several supernova surveys. Some of the systematics are associated with particular surveys, while others are common to all surveys (intristic variation in supernova explosion mechanism or their possible evolution). In the standard approach, systematic errors are estimated by adding a systematic component, σ_{sys}, in quadrature to the statistical error. The amplitude of σ_{sys} is then evaluated so that the χ^2 per degree of freedom for the best fitting cosmological model is unity. However, since in this paper we aim to constrain inhomogeneous cosmological models, and to determine whether or not they are able to provide a successful fit to the cosmological observations, we have decided not to account for possible systematical errors. Indeed, using the procedure described above would allow us to fit the supernovae data with almost any model. On the other hand, we find that the best-fit model of the family of models studied in this section (see Table 2 for the exact values of model parameters) fits supernova data with $\chi^2 = 325.89$ (for 304 degrees of freedom), which means that the model can be ruled out at only the 81.4% level. The overall fit to all three cosmological data sets (BAO+H(z)+Union) is 336.55 (for 314 degrees of freedom), which means that the model can be ruled out at only the 81.7% level. These low values of values of χ^2 per degree of freedom imply that these observational data cannot rule out anti-Copernican models describing a large cosmic depression. Within the parametrization assumed, the best fitted void has a density contrast of $\delta_\rho \approx 4.5$ and a radius of $\sigma \approx 3.2$ Gpc.

We find that the best constraints come from the supernova data set. This is mostly because 304 measurements are available, compared with only 9 for $H(z)$ and just one for BAO. However, as may be seen from the lower left panel of Fig. 3., the $H(z)$ data prefers large voids, and so these data also contribute to constraints on parameter estimates. The weakest constraints come from the BAO measurement — see upper left panel of Fig. 3.

5.2. Cosmic flow models

As above we allow three parameters to vary in the range $H_0 \in [64, 76]$ km s^{-1} Mpc^{-1}, $\sigma \in [0, 6]$ Gpc, and $\delta_H \in [0, 0.4]$. The likelihood distributions for these parameters, based on the BAO+H(z)+Union data sets are presented in Fig. 4. The constraints on the parameters δ_H and σ are shown as contour plots of χ^2 after marginalizing over H_0

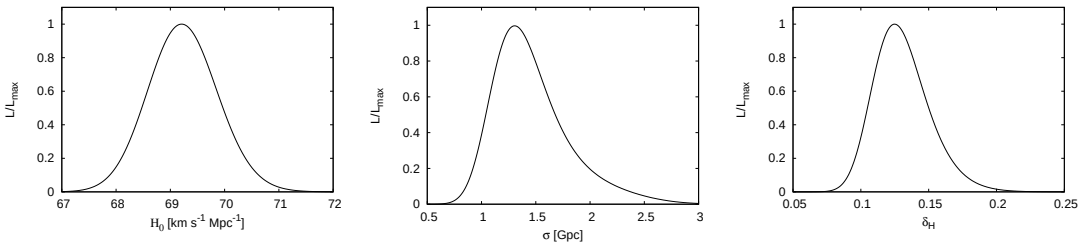

Figure 4. Likelihood profiles for H_0, σ, and δ_ρ based on the BAO+H(z)+Union data sets. *Left* panel: The H_0 likelihood profile obtained after marginalization over σ and δ_ρ. *Center* panel: The σ likelihood profile obtained after marginalization over H_0 and δ_ρ. *Right* panel: The δ_ρ likelihood profile obtained after marginalization over σ and H_0. The means are presented in Table 1.

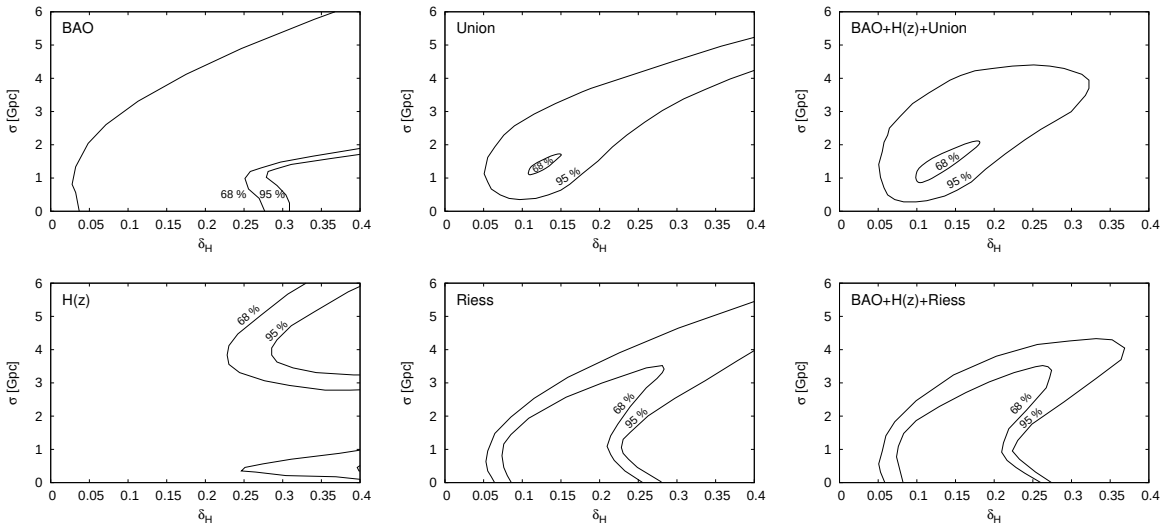

Figure 5. Observational constraints on the parameters of the second family of models (cosmic flow models), shown as contour plots of χ^2 for the model given the data, after marginalizing over H_0. The confidence levels are set assuming a χ^2 distribution. *Upper Left*: constraints from the BAO. *Lower Left*: constraints from H(z). *Upper Center*: constraints from the Union data set. *Lower Center*: constraints from the Riess gold data set. *Upper Right*: joint constraints from the BAO+H(z)+Union data sets. *Lower Right*: joint constraints from the BAO+H(z)+Riess data sets.

in Fig. 5. This family of models provides an even better fit to available observations. The best-fit model fits the data (BAO+H(z)+Union) with $\chi^2 = 317.64$ (for 314 degrees of freedom) which means that the model can be ruled out at only the 56.8% level. The best-fit model has $H_0\delta_H \approx 8.5$ km s^{-1} Mpc^{-1} and $\sigma \approx 1.3$ Gpc. We note that this large scale flow is not compatible with the original Hubble Bubble from Ref. [13] where $H_0\delta_H \approx 4.5$ km s^{-1} Mpc^{-1} and $\sigma \approx 0.1$ Gpc. Indeed, as seen from Fig. 5 the Hubble Bubble can be ruled out at 2σ confidence. However, when the Riess gold data set is used to constrain the model, the Hubble Bubble is only ruled out at the 1-sigma level.

Table 1. Expected values (means) for H_0, σ, and δ_ρ based on the BAO+H(z)+Union data sets.

model	H_0 [km s^{-1} Mpc^{-1}]	σ [Gpc]	δ
cosmic void	$67.62^{+0.49}_{-0.48}$	$2.96^{+0.19}_{-0.45}$	$4.05^{+1.28}_{-1.44}$
cosmic flow	$69.24^{+0.66}_{-0.62}$	$1.46^{+0.55}_{-0.26}$	$0.13^{+0.02}_{-0.01}$

Table 2. Parameters and the χ^2 of the best-fit models based on the BAO+H(z)+Union data sets.

model	H_0 [km s^{-1} Mpc^{-1}]	σ [Gpc]	δ	χ^2	χ^2/dof
cosmic void	67.603	3.119	4.501	336.55	1.07
cosmic flow	69.209	1.327	0.123	317.64	1.01

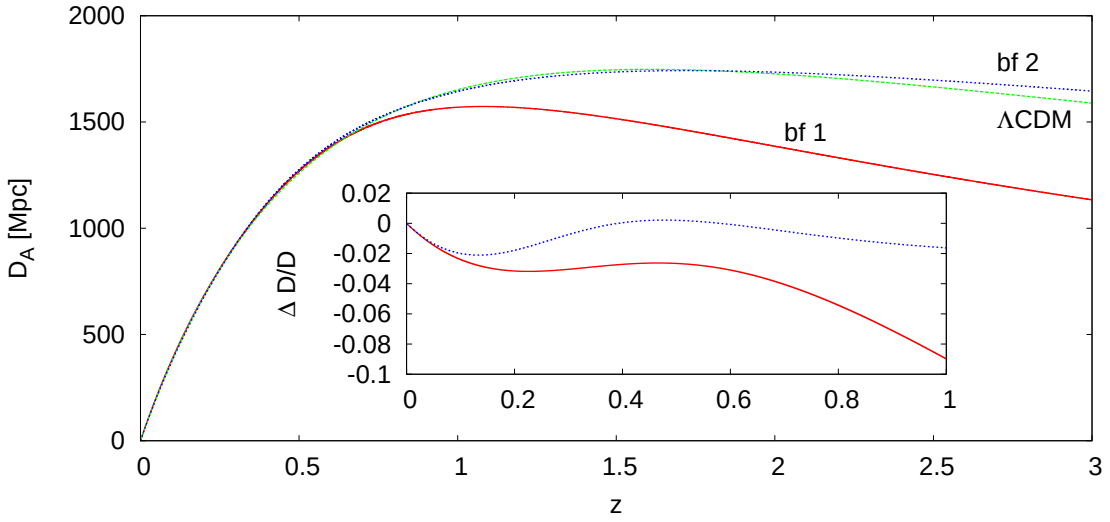

Figure 6. The angular diameter distance as a function of redshift in the ΛCDM model and the best-fit inhomogeneous models (bf 1 – best-fit cosmic void model, bf 2 – best-fit cosmic flow model). The inset presents the absolute distance difference, i.e. $(D - D_{\Lambda\mathrm{CDM}})/D$ (where D is the angular distance either in bf 1 or bf 2 model).

6. Future observational constraints

The previous section showed that very large regions of parameter space for inhomogeneous models can be ruled out by combinations of existing constraints. However, a large scale void model or an ultra-large cosmic flow remain as possible alternatives to dark energy with respect to explaining the apparent acceleration of the Universe. In our analysis we did not consider constraints from the CMB. This

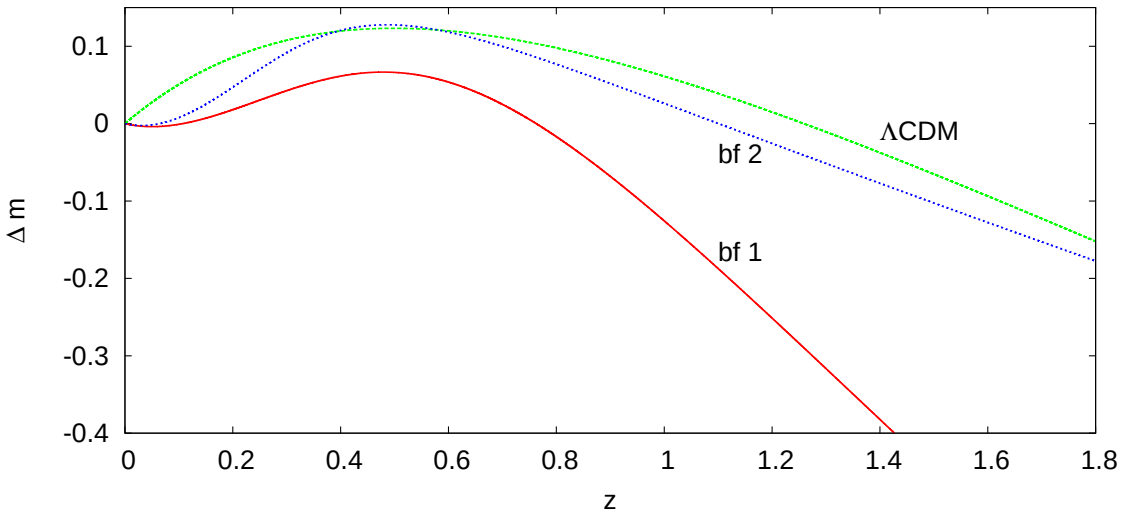

Figure 7. The residual Hubble diagrams for the best-fit void model (bf 1), best-fit cosmic flow model (bf 2), and the ΛCDM model.

is because observations at high redshift ($z \gg 1$) are of limited significance when used to constrain the properties of the local-scale inhomogeneities. Owing to the flexibility of inhomogeneous models we can always assume that our void is surrounded by an overdense or underdense region – there is not need to assume that the Universe consists only of the void of Gpc-radius and everywhere else is homogeneous. Thus, by varying the density of such a ring or its size, every model studied in this paper can be made to fit the distance to the last scattering surface (which is given by the position of the first of the CMB peak). Thus, the high redshift data does not significantly constrain the properties of a local inhomogeneity (see Appendix for more details). To tighten the constraints on the properties of the local Gpc-scale inhomogeneity we need more precise data sets at low redshift which can be directly compared with constraints from existing data sets such as Type-Ia supernovae. Among these observations, the most valuable are those of distance, of the Hubble parameter, or measurements like baryonic acoustic oscillations and the Alcock–Paczyński tests which depend on both the Hubble parameter and distance. For example, precise measurements of a maximum in the angular diameter distance distance would place very tight constraints [21, 22]. This is depicted in Fig. 6 which shows the angular distance as a function of redshift in the ΛCDM model and in the best fitted models for both families of models studied in this paper. The angular distance to $z > 1$ in inhomogeneous void models is distinguishable from the corresponding distance in homogeneous models, at a level larger then 10%. In addition and the position of maximum for model bf 1 is shifted by $\Delta z \approx 0.5$ relative to the ΛCDM model. However, current estimates of the angular distance from SnIa are predominantly at $z < 1$, and are not sufficiently precise to discriminate between models on this basis. Other state of the art the measurements of the distance based on the Sunyaev-Zel'dovich effect are also too imprecise [23]. Another possible test that has been proposed in the literature is

based on the time drift of cosmological redshift, i.e. a measurement of $\dot{z}$ [24]. However, this requires a very precise measurement since the typical amplitude of the effect is $\delta z \sim 10^{-10}$ on a time scale of 10 years [24]. Another possible test was proposed in [25], which relies on studying the consistency relation between the distance on the null cone and the Hubble parameter. Such relation does not hold if the geometry of the Universe differs from the FLRW geometry. Of more immediate utility are methods based on spectral distortions of the CMB power spectrum [26]. These have already been used to put an upper bound of ≈ 1 Gpc for the radius of a local Gpc-scale void [27]. In addition, a study of the kinematic Sunyaev–Zel'dovich effect has recently been used by García-Bellido and Haugbølle [7] to estimate the properties of a local void. This analysis shows that the void permitted by the existing data cannot be larger than ~ 1.5 Gpc. We recall from Sec. 5.1 that a void with $\sigma = 1$ Gpc and $\delta_\rho = 0.95$ fits the data with $\chi^2 = 347.27$, which means that that the model can be rejected at only the 90.5% level, which is insufficient to rule out this possibility. Moreover, cosmic-flow models, although not tested with these type of observations (kSZ effect and spectral distortion), require an inhomogeneity of radius also around 1 Gpc. Therefore, there is a need for future observational constraints to either confirm or rule out the existence of these large inhomogeneities.

Of considerable promise for the future are very precise measurements of supernova in the redshift range of 0.1-0.4 [8]. In this redshift range (see Fig. 7) measurements of over 2000 supernova (for example by the Joint Dark Energy Mission) will be sufficient to reassure existence of such a void. However, in the near future the most promising candidate for testing inhomogeneous cosmological models are BAO measurements. Current measurements of BAO from LRG SDSS (for an up to date status see [28]) already add additional constrains (Figs. 3 and 5). Moreover, the WiggleZ project § will soon measure the dilation distance with accuracy of 2.5% at $z = 0.75$. In the next subsection we show that this forthcoming observation will be sufficient to significantly constrain the inhomogeneous cosmological models.

6.1. BAO constraints

Before proceeding with further analysis, we asses the importance of analysing BAO data using inhomogeneous, rather than FLRW models. For example, when analysing the data in [19] the redshifts of LRG galaxies were translated into comoving coordinates using the flat FLRW model with $\Omega_m = 0.3$, $\Omega_\Lambda = 0.7$, $H_0 = 70$ km s^{-1} Mpc^{-1}. However, if the ΛCDM model is not a good background model of the Universe then such a procedure leads to inaccurate results. The error which arises from this conversion can be estimated from the inset in Fig. 6. As seen at $z = 0.35$, the error in the distance conversion is 3% and 0.3% respectively in cases where the best-fit model from the first (bf 1) and second (bf 2) family of models studied in this paper were chosen as the background rather than the ΛCDM model. These results indicate that while the effect is relatively small,

§ http://wigglez.swin.edu.au

we should be aware that the value D_V at $z = 0.35$ estimated in [19] when using the inhomogeneous model could be different than $D_V = 1370 \pm 64$ Mpc. On the other hand we find that even if this value was change by 5% the results presented in the previous section would still hold. This is because the, as seen from Figs. 3 and 5 the observations of BAO at $z = 0.35$ do not put tight constraints on the inhomogeneous models relative to data. However at higher redshift ($z \approx 1$) the redshift-distance conversion error increases to around 10% for the cosmic void model. Thus, when using forthcoming BAO data to constrain inhomogeneous models one must perform with the whole analyses within the inhomogeneous framework.

In this section we will assume for the sake of argument that such an analysis has been performed. We will also assume that the D_V is equal to the value obtained within the ΛCDM model ($\Omega_m = 0.3$, $\Omega_\Lambda = 0.7$, $H_0 = 70$ km s^{-1} Mpc^{-1}). As in Sec. 5 we set $\sigma \in [0, 6] Gpc$, $\delta_\rho \in [0, 6]$, and $\delta_H \in [0, 0.4]$. However, we tighten H_0 range to $H_0 \in [68, 72]$, because future observational experiments like WiggleZ project will measure the Hubble parameter with 4% precision.

The potential constraints from this BAO experiment around the ΛCDM model are presented in the left panels of Fig. 8. As measurement of the BAO scale at $z = 0.75$ with a precision of 2.5% would rule out most of the parameter space considered for the cosmic depression family of models. A measurement at $z = 0.95$ with 2.5% accuracy would be sufficient to rule out all remaining possibilities in this case at a significance of 3σ.

The second family of models considered in this paper are not tightly constrained by a single BAO measurement at $z = 0.75$. As seen in lower right panel of Fig. 8 even measurements up to redshift 1.75 are not able to rule out this type of model. To rule out all remaining possibilities at a significance of 3σ measurements should be extended beyond $z = 2$.

7. Conclusions

Homogeneous cosmological models which include a dark energy component and which are built on the Copernican Principle have been spectacularly successful in describing a suite of cosmological observations. However, alternatives which replace dark energy with an gigaparsec-scale inhomogeneity have also been postulated as explanations for the apparent acceleration of the Universe. In this paper we have shown that most inhomogeneous anti-Copernican models can already be ruled out by combining current cosmological observations (SNIa, H(z), and BAO). Our model were based on a simple parametrization of an inhomogeneity. We assumed that the inhomogeneity is modeled with a Gaussian-like profile, although other profiles are also possible. For example a similar analysis was recently proposed by García-Bellido and Haugbølle [30] were the inhomogeneity was modeled using a hyperbolic tangent function. Their results also support our conclusion that there is still a range of parameter space that remains consistent with current constraints. As a result the success of Concordance

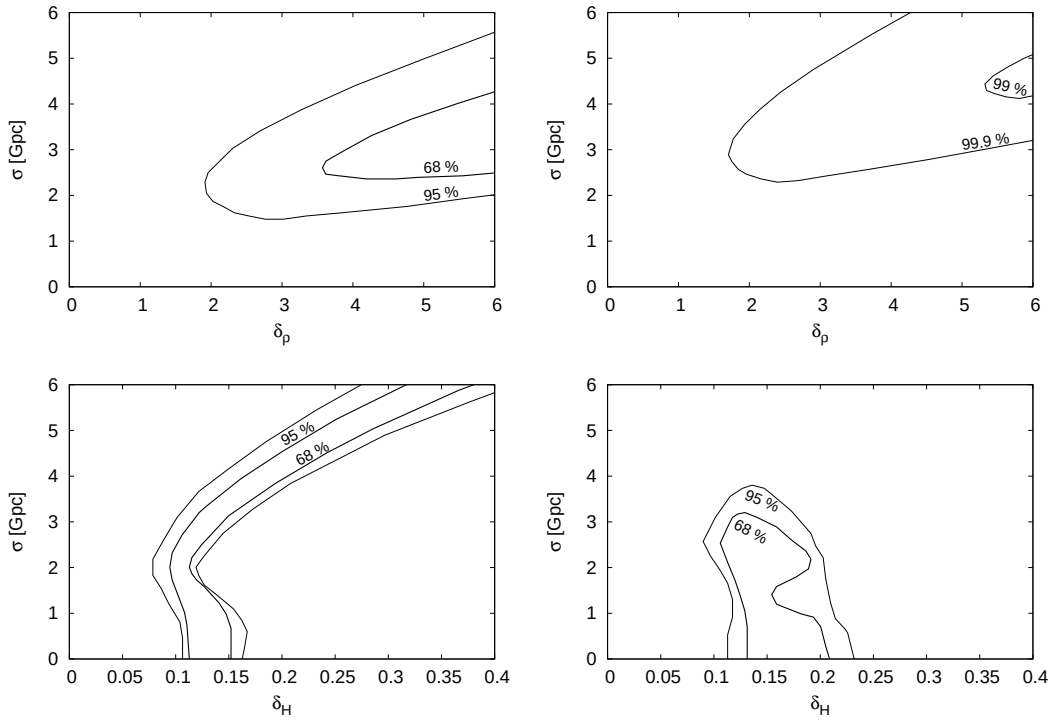

Figure 8. Observational constraints on the parameters of the first family of models, shown as contour plots of χ^2 for the model given the data, after marginalizing over H_0. The confidence levels are set assuming that the value of D_V is the same as in the ΛCDM model and that it is measured with 2.5% precision. *Upper Left*: expected constraints from the BAO at z=0.75 for the first family of models (cosmic void). *Upper Right*: expected constraints from the BAO at z=0.95 for the first family of models (cosmic void). *Lower Left*: expected constraints from the BAO at z=0.75 for the second family of models (cosmic flow). *Lower Right*: expected constraints from the 8 BAO measurements at z=0.35,0.55,0.75,...,1.75.

models cannot be considered as a validation of the Copernican Principle. Forthcoming experiments will be capable of constraining all possible alternatives and will therefore either validate the Copernican Principle or determine the existence of a local Gpc-scale inhomogeneity.

Acknowledgments

This research was supported by the Peter and Patricia Gruber Foundation and the International Astronomical Union (KB) and by the Australian Research Council (JSBW). We thank Aleksandra Kurek for helpful discussions.

Appendix A. Fitting the CMB data with inhomogeneous models

In the standard approach, the CMB temperature fluctuations are analyzed by solving the Boltzmann equation within linear perturbation around the homogeneous and isotropic

FLRW model [31, 32]‖. Within an inhomogeneous background one can proceed with a similar analysis – employing the LT model instead of the FLRW model. Alternatively, if it is assumed that the early Universe (before and up to the last scattering instant) is well described by the FLRW model then the CMB power spectrum can be parametrized by [33]

$$l_m = l_a(m - \phi_m) \tag{A.1}$$

where l_1, l_2, l_3 is a position of the first, second and third peak, and

$$l_a = \pi \frac{R}{r_s}, \tag{A.2}$$

where R is a comoving distance to the last scattering surface and r_s is a size of the sound horizon at the last scattering instant. The sound horizon depends on $\Omega_b,\ \Omega_m,\ \Omega_\gamma$, and h (where $\Omega_b,\ \Omega_m,\ \Omega_\gamma$ are ratios of baryon, mater and radiation energy density respectively to the critical energy density evaluated at the current instant and h is equal to H/100 km s^{-1} Mpc^{-1}). The size of the sound horizon can be calculated accordingly to formulae given in [34]. The function ϕ_m depends on $\Omega_b,\ \Omega_m,\ h,\ n_s$, and the energy density of dark energy (n_s is the spectral index). The exact form of ϕ_m is given in [33]. The Ω_m and h are given by a ratio ρ/ρ_{cr} and $H/(100$ km s^{-1} Mpc$^{-1})$ at the last scattering surface (evaluated for the current instant).

In this appendix we will present a fit to the CMB data using the above formula. Let us consider four models

- model A1:
  $\rho(t_0, r) = \rho_b \left[1 + 1.45 - 1.45 \exp\left(-\frac{\ell^2}{0.75^2}\right)\right]$,
  $t_B = 0, \quad \Omega_b = 0.0445, \quad n_s = 1,$
  where $\ell = r/Gpc$.
- model A1+ring:
  $\rho(t_0, r) = \rho_b \left[1 + 1.45 - 1.45 \exp\left(-\frac{\ell^2}{0.75^2}\right) - 1.75 \exp\left\{-\left(\frac{\ell - 5.64}{0.926}\right)^2\right\}\right]$,
  $t_B = 0, \quad \Omega_b = 0.08, \quad n_s = 0.963.$
- model A2
  $\rho(t_0, r) = \rho_b \left[3.33 + 1.4 \exp\left(-\frac{\ell^2}{0.75^2}\right)\right]$,
  $t_B = 0, \quad \Omega_b = 0.0445, \quad n_s = 1.$
- model A2+ring:
  $\rho(t_0, r) = \rho_b \left[3.33 + 1.4 \exp\left(-\frac{\ell^2}{0.75^2}\right) + 0.08 \exp\left\{-\left(\frac{\ell - 7.5}{0.965}\right)^2\right\}\right]$,
  $t_B = 0, \quad \Omega_b = 0.07, \quad n_s = 0.963.$

The density distributions of these models are presented in Fig. A1. The fit to positions of the CMB peaks is presented in Table Appendix A. As can be seen, model

‖ This approach is implemented in such codes like CMBFAST (http://www.cfa.harvard.edu/∼mzaldarr/CMBFAST/cmbfast.html), CAMB (http://www.camb.info/), or CMBEASY (http://www.cmbeasy.org/).

Table A1. CMB fit

Model	First peak	Second peak	Third peak
A1	177.34	414.08	627.19
A2	216.59	503.37	754.28
A1 + ring	220.46	530.38	800.19
A2 + ring	220.43	530.51	779.76
WMAP [35, 1]	220.8 ± 0.7	530.9 ± 3.8	$700 - 1000$

A1 does not fit the observed CMB power spectrum. However, we can modify the density distribution is such a way (by adding an underdense ring) that the CMB peaks can be reproduced – model A1+ring. In models where density increases up to some distance from the origin (local void type of models) a satisfactory fit to the first peak of CMB power spectrum (i.e. distance to the last scattering instant) can be obtained if the mass of the universe is decreased. This decrease can be obtained either by having a local void of a larger radius (as in [6] where $R \approx 2.5$ Gpc), or by having an addition underdense ring between local void and the last scattering surface.

On the other hand, it is not only the mass that is important. To show this let us consider model A2. In model A2 the density decreases up to some distance from the origin. In this configuration we can also obtain a good fit to the position of the first peak if we increase the mass of the universe.

The positions of other peaks strongly depend on Ω_b. To obtain a good fit to the positions of other peaks in our model we need to increase the value of Ω_b beyond the value that is consistent with observation of light elements in the local Universe ($\Omega_b = 0.0445$ [36]) to $\Omega_b = 0.08$. However, due to the lower expansion rate at large distances, the physical baryon density $\Omega_b h^2$ remains is close to the observed value, i.e. 0.0198 and 0.0212 for models A1+ring and A2+ring respectively.

The above results suggest that almost every model can be modified in such a way that a good fit to CMB power spectrum data can be obtained. Models A1 and A2 are very different and yet after some modifications they are both able to fit the CMB data. Thus, the CMB data does not strongly constrain the properties of the local Gpc void. Each model for the local scale void considered in this paper can be modify in such a way (by adding one or two rings between a local void and the last scattering surface) so that the CMB power spectrum is recovered.

References

[1] Hinshaw G *et al* 2008 submitted to *Astrophys. J. Suppl. Ser.* (*Preprint* arXiv:0803.0732)
[2] Tegmark M *et al* 2006 *Phys. Rev.* D **74** 123507
[3] Percival W J *et al* 2002 *Mon. Not. Roy. Astr. Soc.* **337** 1068
[4] Dąbrowski M P and Hendry M A 1998 *Astrophys. J.* **498**, 67; Célérier M N 2000 *Astron. Astrophys.* **353** 63; Iguchi H, Nakamura T and Nakao K 2002 *Prog. Theor. Phys.* **108** 809; Chung D J H and Romano A E 2006 *Phys Rev.* D **74** 103507; Alnes H and Amarzguioui M

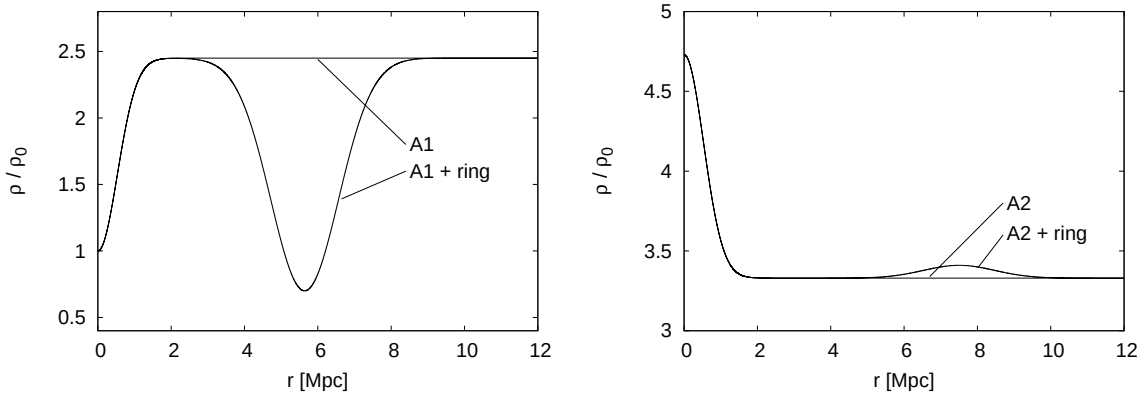

Figure A1. Density distribution at the current instant for models A1, A2, A1+ring, A2+ring.

2007 *Phys. Rev.* D **75** 023506; Enqvist K and Mattsson T 2007 *J. Cosmol. Astropart. Phys.* JCAP07(2007)02019; Biswas T, Mansouri R and Notari A 2007 *J. Cosmol. Astropart. Phys.* JCAP12(2007)017; Brouzakis N, Tetradis N and Tzavara E 2007 *J. Cosmol. Astropart. Phys.* JCAP0702(2007)013; Brouzakis N, Tetradis N and Tzavara E 2008 *J. Cosmol. Astropart. Phys.* JCAP0804(2008)008; Marra V, Kolb E W, Matarrese S and Riotto A 2007 *Phys. Rev.* D **76** 123004; Biswas T and Notari A 2008 *J. Cosmol. Astropart. Phys.* JCAP06(2008)021; Bolejko K 2008 *PMC Physics* PMCA02(2008)01 (*Preprint* astro-ph/0512103); Enqvist K 2008 *Gen. Rel. Grav.* **40** 451; Khosravi Sh, Kourkchi E, Mansouri R and Akrami Y 2008 *Gen. Rel. Grav.* **40** 1047; Yoo C-M, Kai T and Nakao K-i 2008 *Preprint* arXiv:0807.0932

[5] Godłowski W, Stelmach J and Szydłowski M 2004 *Class. Q. Grav.* **21** 3953; Alnes H. and Amarzguioui M and Grøn Ø 2006 *Phys.Rev.* D **73** 083519; Alnes H and Amarzguioui M 2006 *Phys. Rev.* D **74** 103520; Alexander S, Biswas T, Notari A and Vaid D 2007 *Preprint* arXiv:0712.0370

[6] García-Bellido J and Haugbølle T 2008 *J. Cosmol. Astropart. Phys.* JCAP04(2008)03

[7] García-Bellido J and Haugbølle T 2008 *J. Cosmol. Astropart. Phys.* JCAP09(2008)016

[8] Clifton T, Ferreira P G and Land K *Preprint* arXiv:0807.1443

[9] Célérier M N 2007 *New Adv. Phys.* **1** 29

[10] Mustapha N, Hellaby C and Ellis G F R 1997 *Mon. Not. R. Astron. Soc.* **292** 817

[11] Lemaître G 1933 *Ann. Soc. Sci. Bruxelles* A **53** 51 (1933) (reprinted in 1997 *Gen. Rel. Grav.* **29** 641); Tolman R C 1934 *Proc. Nat. Acad. Sci. USA* **20** 169 (reprinted in 1997 *Gen. Rel. Grav.* **29** 935)

[12] Hellaby C and Lake K 1985 *Astrophys. J.* **290** 381; Hellaby C and Lake K 1986 *Astrophys. J.* **300** 461

[13] Jha S, Riess A G and Kirshner R P 2007 *Astrophys. J.* **659** 122

[14] Mustapha N and Hellaby C 2001 *Gen. Rel. Grav.* **33** 455

[15] Freedman W L et al. 2001 *Astrophys. J.* **553** 47

[16] Bondi H 1947 *Mon. Not. Roy. Astr. Soc.* **107** 410

[17] Kowalski M et al. 2008 *Preprint* arXiv:0804.4142

[18] Riess A G et al. 2007 *Astrophys. J.* **659** 98

[19] Eisenstein D J et al. 2005 *Astrophys. J.* **633** 560

[20] Simon J, Verde L and Jimenez R 2005 *Phys. Rev.* D **71** 123001

[21] Hellaby C 2006 *Mon. Not. Roy. Astr. Soc.* **370** 239

[22] Araújo M E and Stoeger W R 2007 *Preprint* arXiv:0705.1846

[23] Bonamente M et al. 2006 *Astrophys. J.* **647** 25

[24] Uzan J-P, Clarkson C and Ellis G F R 2008 *Phys. Rev. Lett.* **100** 191303
[25] Clarkson C, Bassett B and Lu T H-C 2008 *Phys. Rev. Lett.* **101** 011301
[26] Goodman J 1995 *Phys. Rev.* D **52** 1821
[27] Caldwell R R and Stebbins A 2008 *Phys. Rev. Lett.* **100** 191302
[28] Gaztanaga E, Cabre A and Hui L 2008 *Preprint* arXiv:0807.3551
[29] Bolejko K and Lasky P D 2008 *Mon. Not. R. Astron. Soc.* **391** L59
[30] García-Bellido J and Haugbølle T 2008 *Preprint* arXiv:0810.4939
[31] Seljak U and Zaldarriaga M 1996 *Astrophys. J.* **469** 437
[32] Seljak U, Sugiyama N, White M and Zaldarriaga M 2003 *Phys. Rev.* D **68** 083507
[33] Doran M and Lilley M 2002 *Mon. Not. R. Astron. Soc.* **330** 965
[34] Eisenstein D and Hu W 1998 *Astrophys. J.* **496** 605
[35] Hinshaw G *et al* 2007 *Astrophys. J. Suppl. Ser.* **170** 288
[36] Cyburt R H 2004 *Phys. Rev.* D **70** 023505